47

A Comparison of the Failure Pressure as Predicted by Finite Element Stress Analysis with the Results of Full Scale Burst Tests on GRP Flanges

A. MUSCATI AND R. BRADFORD

Central Electricity Generating Board (South Western Region), Bedminster Down, Bridgwater Road, Bristol BS13 8AN, England

ABSTRACT

The burst pressure from full scale burst tests on GRP pipes with integral GRP flanges is compared with the predicted failure pressure using glass content analysis and material strength data for the different composite layers. Two theoretical models were used to predict the failure load; a simple analytical solution for a plain pipe and a detailed finite element stress analysis including the flange geometry and loading. In both cases, the failure pressure was generally overestimated and it is suggested that this may be due to difficulties in construction resulting in the composite layers close to the flange having inferior strength as compared with a basic pipe with the same glass content.

1. INTRODUCTION

An experimental programme of full scale burst tests was carried out to assess the long term integrity of a glass reinforced plastic (GRP) pipe installation. The results of earlier burst tests[1] showed the flanges to have a much lower strength than the basic pipes. This was attributed to the difficulties in construction resulting in inadequate roving reinforcement at the flanged joint.

Further burst tests were carried out after the publication of Ref. 1 to test flanges extracted from the installation. Using the results of all the burst tests, an attempt was then made to correlate the burst pressure with the glass content for some of the test specimens using both analytical and finite

Results

element stress analysis
these flanges on site
scale flanged joints,
Details of the expe
here with the emphas
failure pressures.

2. PIPE

A full description of
Basically, it is a GRP
unplasticised polyvin
strand mat (CSM)
orientated glass fibr
directions whilst the

C.S.M
FLANGE OU
SURFACE

FIG. 1.

Nominal properties[a]

Layer	T
UPVC	
CSM	
Rovings	

[a] Poisson's ratio assur
[b] Locally thicker near
glass content of 3·36

element stress analysis techniques. Also, a practical method for reinforcing these flanges on site was developed in the laboratory and applied to full scale flanged joints, which were pressure tested to failure.

Details of the experimental programme and the stress analysis are given here with the emphasis on a comparison between the predicted and actual failure pressures.

2. PIPE GEOMETRY AND CONSTRUCTION

A full description of the pipe and flange construction is given in Ref. 1. Basically, it is a GRP pipe with integral GRP flanges. The pipe is lined with unplasticised polyvinyl chloride (UPVC) and made up of layers of chopped strand mat (CSM) and rovings. The CSM layers consist of randomly orientated glass fibres providing reinforcement in both axial and hoop directions whilst the rovings have unidirectional fibres along the hoop

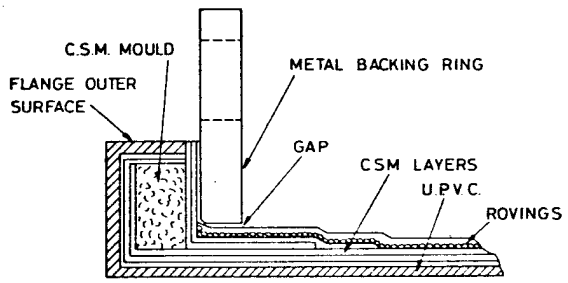

FIG. 1. A schematic diagram for the flange construction.

TABLE 1
Nominal properties[a] of different layers of the composite pipe (I.D. 304 mm)

Layer	Thickness (mm)	Young's modulus (N/mm^2)	UTS (N/mm^2)	Designed glass content kg/m^2
UPVC	3·1	$2{\cdot}76 \times 10^3$	48	
CSM	4·0[b]	$6{\cdot}41 \times 10^3$	93	2·14
Rovings	3·2	$3{\cdot}45 \times 10^4$	827	3·89

[a] Poisson's ratio assumed to be 0·4.
[b] Locally thicker near flange (up to 6·3 mm) corresponding to an increased designed glass content of 3·36 kg/m^2.

direction only. Details of the dimensions and material properties, as supplied by the manufacturers, are given in Table 1 for each layer. A schematic diagram showing the flange construction is shown in Fig. 1.

3. EXPERIMENTAL WORK

3.1. The Burst Tests

Details of the testing rig and the results of the earlier tests are given in Ref. 1. In brief, the specimen is a full scale pipe with an integral GRP flange at each end bolted to a steel plate. The specimens were tested inside a cage which can provide practically full axial restraint.

Table 2 gives the results for all the tests including those published earlier. Note that some of the test results are not relevant for the comparison with the theoretical calculations but are given here for completeness.

TABLE 2
Results of burst tests

Specimen no.	Type[a]	End conditions	Failure pressure (N/mm^2)	Description	Crack position
1	A	fully restrained	4·5	burst	at flange
2	A	fully restrained	5·4	leak	at flange
3	A	fully restrained	5·4	leak	at flange
4[b]	A	fully restrained	2·4	leak	at flange
			11·7	burst	
5	C	7·6 mm axial gap	3·4	burst	at flange
6	A	7·6 mm axial gap	5·2	burst	at flange
7	C	7·6 mm axial gap	1·7	burst	at flange
8	E	7·6 mm axial gap	3·96	burst	at pipe joint
9	B	fully restrained	3·63	leak	at flange
10	E	fully restrained	4·64	burst	at pipe joint
11	B	2·5 mm axial gap	4·51	burst	at flange
12	D	fully restrained	6·20	burst	at flange
13	D	free	5·44	burst	at flange
14	B	2·5 mm axial gap	5·57	burst	at flange

[a] Type A: Pipes manufactured for testing but intended to simulate site flanges. Type B: Pipes extracted from site. Type C: Specially manufactured pipes with substandard flanges. Type D: Specially manufactured with strong flanges. Type E: Failure occurred at the pipe away from the flange.
[b] Specimen No. 4 is 250 mm diameter.

3.2. Glass Analysis

Glass content anal
10 of them are releva
The procedure was si
the remaining glass
pressure based on th

In two specimens
joint in the pipe awa
carried out on two sa
of the remaining eigh
the area of interest is
glass analysis showe
decreases as the GR
therefore based on
adjacent to the GRI

Table 3 gives the
correspond to the m

Specimen no.	CSM	I
1	3·04	
2	2·87	
3	3·36	
5	2·80	
6	4·03	
7a[c]	1·44	
7b	1·09	
8[d]	1·86	
10[d]	1·97	
11	1·93	
14	1·94	

[a] The predicted failure
[b] Although these crack
changed after it propag
[c] a and b are top and bo
flange.
[d] Data refer to butt joi

3.2. Glass Analysis

Glass content analysis was carried out on most of the specimens but only 10 of them are relevant for the comparison with the theoretical predictions. The procedure was simply to burn the polyester resin in a furnace and weigh the remaining glass. The results were then used to predict the failure pressure based on the materials data and stress calculations.

In two specimens (Nos. 8 and 10), failure occurred at a hand-laid butt joint in the pipe away from the flange. In this case, the glass analysis was carried out on two samples for each specimen taken at the butt joint. In each of the remaining eight specimens, failure occurred at one of the flanges and the area of interest is the pipe immediately adjacent to the failed flange. The glass analysis showed that the glass content for the rovings in the pipe decreases as the GRP flange is approached. The stress calculations were therefore based on the glass content analysis of the pipe immediately adjacent to the GRP flange, up to about 20 mm from it.

Table 3 gives the relevant results of the glass content analysis which correspond to the minimum values.

TABLE 3
Details of glass analysis (kg/m^2)

Specimen no.	CSM	Rovings		Failure pressure (N/mm^2)		Crack orientation
		Hoop	Axial	Actual	Predicted[a]	
1	3·04	2·11		4·5	9·1	axial[b]
2	2·87	1·63		5·4	7·8	axial
3	3·36	2·61		5·4	10·6	axial
5	2·80	0		3·4	4·1	axial[b]
6	4·03	0		5·2	5·4	axial[b]
7a[c]	1·44	0·19			2·9	
7b	1·09	0·83		1·7	3·6	circumferential
8[d]	1·86	0·6	4·45	4·0	4·2	axial
10[d]	1·97	0·6	4·67	4·6	4·3	axial
11	1·93	1·90		4·5	6·9	axial[b]
14	1·94	2·15		6·0	7·4	axial[b]

[a] The predicted failure pressure was based on the analytical solution.
[b] Although these cracks initiated in the axial direction the crack orientation changed after it propagated away from the flange to a circumferential crack.
[c] a and b are top and bottom flanges, the crack from the burst test was at the bottom flange.
[d] Data refer to butt joint away from the flange.

4. STRESS ANALYSIS

4.1. Analytical Solution

A simple analytical solution, for the stresses in different layers of a composite pipe under pressure, may be obtained using the properties of each layer. Such a solution is given in the appendix for the present pipe under both fully restrained and free end conditions. Note that this analysis ignores the flange geometry and only considers a composite pipe. This is applicable to specimens Nos. 8 and 10 where failure occurred at the composite pipe. However, for the remaining specimens the failure was at the flange but the analysis treats the pipe adjacent to the flange in a similar manner to the basic pipe, ignoring the flange geometry.

In using the solution given in the appendix to predict the failure pressure, the following points should be noted:

(1) Failure was assumed to occur when the maximum principal stress in any layer exceeded the ultimate tensile strength (UTS) of the material. For all these specimens, the critical values correspond to the hoop stress in the CSM layer.

(2) In the majority of the burst tests considered, an axial gap was left between the specimen and the cage resulting in only a partial axial restraint. For the purpose of the calculations, the end conditions were assumed to be free up to the pressure necessary to close the gap. This pressure was found from the axial stiffness of the specimen which was determined experimentally to be about 0·8 N/mm^2 per mm. Once the gap is closed the cage was assumed to provide full axial restraint.

(3) The thickness of the CSM and roving layers was calculated from the data given in Table 1 for the basic pipe and the results of glass content analysis in Table 3. This was simply done by scaling the thickness by the ratio of the glass contents as compared to the basic pipe.

The calculated failure pressures based on the above procedure are given in Table 3 and compared with the actual failure pressures.

It is interesting to note that the agreement between the calculated and actual failure pressures is very good for specimens Nos. 8 and 10 (within $\pm 10\%$) where failure occurred away from the flange. However, for the remainder of the specimens, the calculations tend to overestimate the failure pressure by a factor of up to two even though the agreement for some of the specimens is quite good, e.g. Nos. 5 and 6. At this stage, it was difficult

Resu

to judge whether th
pressure is due to th
or simply a functio
solution using finit
model the actual fla

4.2. Finite Element

The 'plain pipe' m
are given in Table 3,
geometry, and (b)
addition, the effects
taken into account.

4.2.1. Method of an

The computer p
programs. An outlir
scale in Fig. 2 and
refinement in this re
isoparametric eleme
pipe is modelled, the
backing ring and b
consists of five differ
and a filler for the
3·5 × 10^3 N/mm^2.

The only medium
that this analysis wa
not available in Bl
decoupling the axia
layers. Since the lay
no axial stresses cai

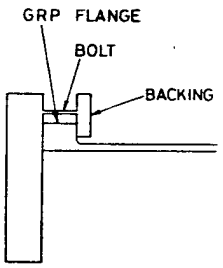

Fi

to judge whether this difference between the actual and calculated failure pressure is due to the geometrical approximations in the analytical solution or simply a function of scatter in material properties. A more accurate solution using finite element stress analysis was therefore attempted, to model the actual flange geometry.

4.2. Finite Element Analysis

The 'plain pipe' model outlined in the appendix, and whose predictions are given in Table 3, may be improved by taking into account; (a) the flange geometry, and (b) stresses arising other than from pressurisation. In addition, the effects of anisotropy and inhomogeneity must clearly also be taken into account.

4.2.1. Method of analysis

The computer programs used were BERSAFE[2] and its associated programs. An outline of the boundary of the mesh employed is shown to scale in Fig. 2 and the flange region is shown in detail in Fig. 3. The refinement in this region is considerable. The elements are axisymmetric, isoparametric elements with 16 degrees of freedom (8 nodes). Only half the pipe is modelled, the remainder being symmetrical. The steel backing plate, backing ring and bolts are included in the mesh. The mesh therefore consists of five different materials, these being steel, UPVC, CSM, rovings and a filler for the flange body. The latter has a Young's modulus of $3{\cdot}5 \times 10^3$ N/mm^2.

The only medium treated as anisotropic was the roving layer. At the time that this analysis was carried out, axisymmetric anisotropic elements were not available in BERSAFE and so the anisotropy was modelled by decoupling the axial degrees of freedom between the roving and CSM layers. Since the layer of rovings is then free to slide axially along the pipe, no axial stresses can occur in the rovings. Note that for convenience in

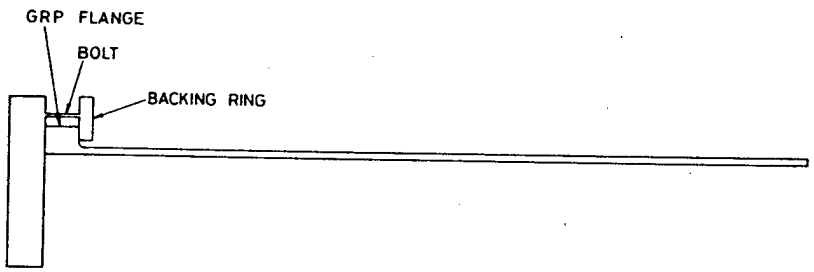

FIG. 2. Scale plot of the outline of the mesh.

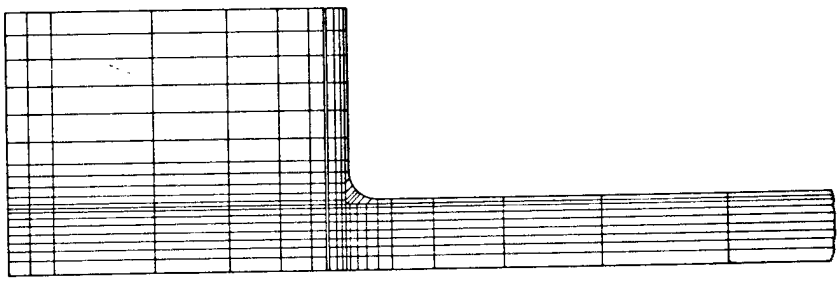

FIG. 3. Scale plot of the mesh in the flange region showing individual elements.

defining the mesh the roving layer has been modelled as being thinner than its actual value, but with an appropriately scaled Young's modulus. Since hoop bending stresses cannot occur, this is of no consequence.

The paucity of rovings close to the flange was modelled by omitting the initial roving elements up to a distance of 74 mm from the back face of the flange. This is admittedly a crude procedure, in that the specimens actually exhibited a gradual increase in the amount of rovings with axial position. Consideration of the extent of roving depletion along the axial length for each specimen, implies that the model is a good approximation for specimen 6, whilst being optimistic for specimens 5 and 7. For the remaining specimens, however, the model is clearly pessimistic, i.e. the model should underestimate the failure pressure, since the actual roving depletion was not as severe as that of our model.

Finally note that the backing plate and the flange are topologically distinct, so that a gap may open between them.

4.2.2. Loadings

Three loads were applied separately to the mesh, as described below:

(1) Pressure was applied to the cylindrical surface with the ends of the mesh axially restrained. This corresponds to the 'restrained' case of the appendix. The front face of the flange is left radially free during this loading. The radial freedom of the flange is further ensured during this loading by assigning zero stiffness to the 'steel' sealing arrangement.

(2) An axial displacement of the pipe of 7·6 mm was simulated by applying half this displacement to the steel backing plate whilst axially restraining the plane of symmetry.

(3) A pressure equivalent to the bolt load due to tightening was applied to the steel backing ring at the bolt radius.

Re

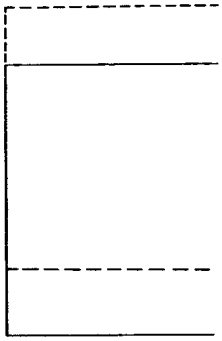

FIG. 4. Deformation
Scale ×

These loads were a
and to the mesh w
assumed throughc

4.2.3. Results

A brief summa
follows:

(1) For pressu
that axial
exaggerat
flange is b
contrast t
rovings.
correspon

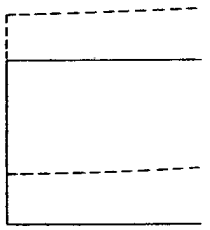

FIG. 5. Deformatio
Scale

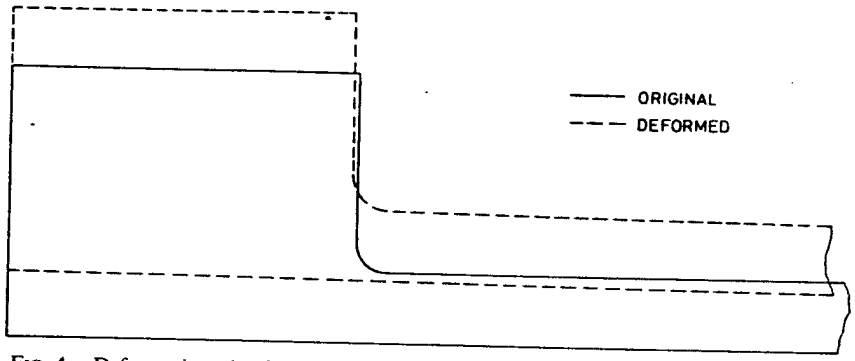

FIG. 4. Deformation plot for the mesh with complete rovings (pressure load, 1 N/mm²). Scale × 2·41 for mesh and additional × 50 for displacement.

These loads were applied both to the mesh representing the as-designed pipe and to the mesh without the initial 74 mm of rovings. Linear elasticity was assumed throughout and hence the effects of combined loads are additive.

4.2.3. Results

A brief summary of the results of the finite element analysis are as follows:

(1) For pressure loading only and with all rovings present it was found that axial bending stresses were absent. This is illustrated by the exaggerated displacement plot of Fig. 4. The radial stiffness of the flange is balanced by the radial stiffness of the rovings. This is in contrast to the result obtained from the mesh without the initial rovings, the displacement plot being shown in Fig. 5. The corresponding stresses in the CSM layer are shown in Fig. 6 for unit

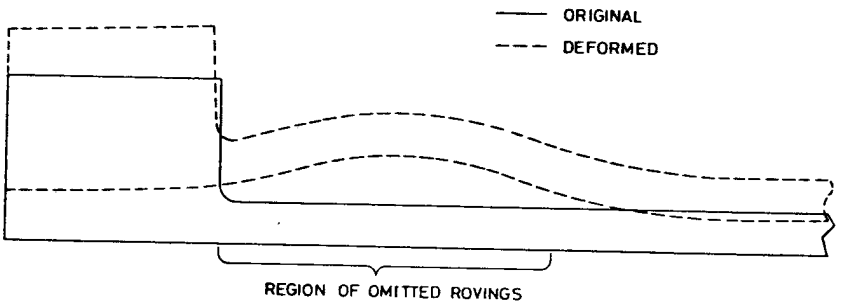

FIG. 5. Deformation plot for the mesh without initial rovings (pressure load, 1 N/mm²). Scale × 1·48 for mesh and additional × 50 for displacement.

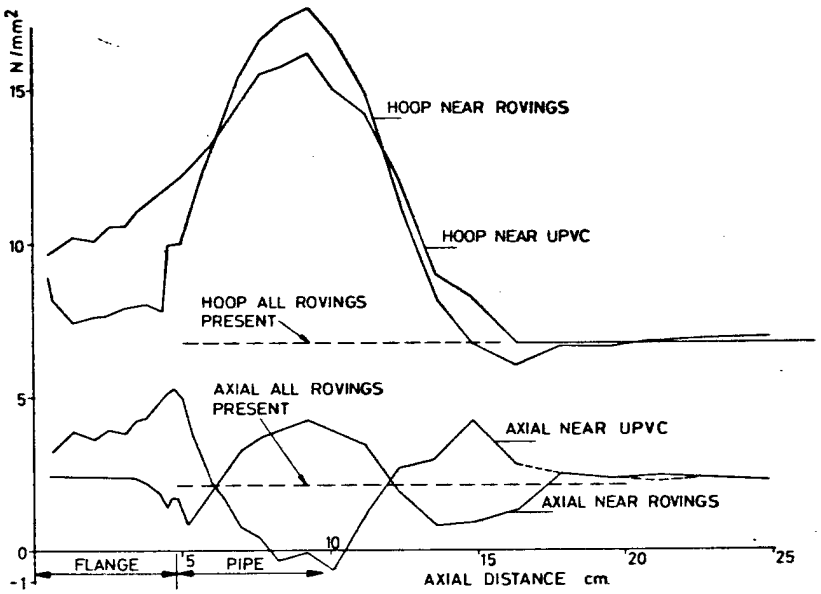

FIG. 6. CSM stresses (pressure load, 1 N/mm²), initial rovings missing.

pressure (1 N/mm²). The increase in the hoop stress caused by the absence of the rovings is clearly considerable. The axial bending stresses which occur are sufficiently small such that the hoop stress is the dominant effect.

(2) The axial displacement load causes compressive stresses in the rovings. The CSM and UPVC stresses, other than in the flange body, for the as-designed pipe are:

CSM 18·9 N/mm² (axial), 5·4 N/mm² (hoop)
UPVC 9·1 N/mm² (axial), 2·6 N/mm² (hoop)

Slight changes from these values occur when the initial rovings are omitted. In particular the hoop stresses near the flange decrease when the rovings are omitted.

(3) The stresses due to bolt loading may be up to 6 N/mm² in the body of the flange but are small in the pipe itself, typically 1 N/mm².

4.2.4. Estimate of the failure pressure

To estimate the failure pressure, the stresses resulting from the three loading cases are added together and each component of stress for each

medium is compared with the UTS given in Table 1. Moreover, this must be done at several characteristic axial positions, since the stresses vary with position. This leads to the following conclusions:

(1) The enhanced CSM hoop stress of Fig. 6 dominates, and it is concluded that this stress component leads to failure.
(2) On the basis of the data of Table 1 failure pressures of 5·0 N/mm^2 (with axial displacement), or 5·2 N/mm^2 (fully restrained) are estimated.
(3) The bolt loading has negligible effect on the failure pressure, whereas the axial displacement reduces the failure pressure by about 4%.

4.2.5. Discussion of the analysis

The finite element analysis models a specimen of CSM glass content of 3·36 kg/m^2 with and without rovings. Taking the case of no rovings and full axial restraint, the simple analytical method described earlier would predict a failure pressure of 4·7 N/mm^2, (11% lower than the finite element prediction). The main conclusion of our finite element analysis is therefore to validate the assumptions made in the simplistic analytic model. The apparently complicating features of the flange geometry and the extra loading due to bolt tightening do not lead to changes in the estimated failure pressure. The fact that the rovings are omitted only for a 74 mm length in the finite element model, whilst the simple method assumes a plain pipe with the rovings missing along its entire length, explains the small difference in the predicted failure pressures.

The finite element analysis has therefore failed to improve the agreement between the predicted and observed failure pressures quoted in Table 3. Rather it has confirmed that the predicted failure pressures are slightly on the low side. In as far as this analysis is believed to be complete, it may be concluded that the disparity between predicted and actual failure pressures is a result of the material data or the failure criterion employed. The disparities cannot be explained in terms of simple material scatter since the burst pressures are consistently lower than the predicted values. This points to a greater preponderance of inherent weaknesses in the tested pipes than in the specimens used in the tensile tests to deduce the data of Table 1. This may be either a consequence of the geometry of the flange leading to poorer lay-up and hence a greater number of voids, etc., per unit volume, or simply a statistical effect due to the larger volume of material under stresses of failure magnitude in the pipes as compared with the tensile tests.

5. REINFORCEMENT OF SITE FLANGES

Fortunately, although the results of the burst tests showed that the GRP flanges had inadequate strength as compared to the design calculations, they were still considered acceptable under the operating conditions. This is mainly because the system was operated at a much reduced pressure (40% below design). Nevertheless, it was still necessary to develop a reinforcement technique for application on site should the system be uprated to the design conditions.

Two reinforcement techniques (A and B) were developed in the laboratory and applied to full scale pipe specimens with flanged joints. These specimens were pressure tested to failure to determine the effect of the reinforcement.

(A) In this case, the approach was to constrain the radial displacement of the flange by using GRP blocks placed on the flange outer surface between the flange bolts (see Fig. 1). These blocks were held in position by a metal split ring which provided the radial constraint. The two halves of the split ring were joined together by two bolts which were tightened up sufficiently to hold the assembly without imposing a significant preload on the flange.

(B) The objective of the second reinforcement technique was to compensate for the lack of sufficient rovings in the pipe adjacent to the flange by providing additional restraint at this position. The method was to inject epoxy resin to fill the gap between the backing ring and the flange (see Fig. 1) so that the backing ring can provide the required reinforcement. This technique was applied to the test specimen with the flange joints assembled and bolted, to simulate site conditions. The main problem was to find a suitable resin that could be used to fill a variable gap (0·25 mm to 3·0 mm), remaining in the gap until it hardens. After a number of trials, the method used was as follows: A standard high pressure grease gun with a specially made flat nozzle was used to inject the resin into the gap. The compound used was a commercial epoxy resin made by CIBA-GEIGY consisting of a resin, 'AV138', and a hardener, 'HV998', the ratio in weight of resin to hardener being 2·5.

A total of four burst tests were carried out, one on a standard specimen without reinforcement, two on specimens with reinforcements of type A and one on a specimen with both types of reinforcements, A and B. The use of reinforcement A alone increased the burst pressure at the flange by a

small amount (15 %) but the application of both reinforcement techniques resulted in an increase in the burst pressure by a factor of approximately two. The latter was therefore recommended should the system be uprated to the design conditions.

6. CONCLUSIONS

A study of the results of the full scale burst tests together with the associated theoretical analysis leads to the following conclusions.

(1) It is possible to model the anisotropic properties of the rovings in the finite element analysis by using isotropic elements but partially decoupling along the boundary nodes of the roving layer.
(2) The lack of sufficient rovings in the pipe adjacent to the flange can cause a serious reduction in the burst pressure.
(3) The local bending stresses resulting from the flange geometry and loading has little effect on the burst pressure even though it can cause a significant increase in the axial stress.
(4) Both finite element and simple analytical solutions tend to overestimate the failure pressure. It is suggested that this is mainly due to the difficulties in construction resulting in a reduction in the strength of the different composite layers in the pipe adjacent to the flange as compared to a basic pipe with the same glass contents.

The above conclusions are only applicable to the particular geometry and loading conditions described in the present paper. The last conclusion, however, implies some caution is needed in assessing the load-bearing capacity of GRP structures.

7. ACKNOWLEDGEMENT

The permission of the Director General of the Central Electricity Generating Board, South Western Region for publication of this paper is acknowledged.

8. REFERENCES

1. MUSCATI, A. and BLOMFIELD, J. A., Full scale burst tests on GRP pipes. In: *Designing with fibre reinforced materials*, London and New York, Mechanical Engineering Publication Ltd for the Institution of Mech. Engineers, 1977.
2. HELLEN, T. K. and PROTHEROE, S. E., BERSAFE finite element system, *Computer Aided Design*, **6** (1974) 15–24.

APPENDIX: STRESS ANALYSIS FOR TEST SPECIMEN (NOMINAL PIPE)

Notation

P pressure
D pipe diameter
E Young's modulus
ν Poisson's ratio
t thickness of different layers
ε strain
σ stress

Subscripts

1 UPVC
2 CSM
3 rovings circumferential
x hoop direction
y axial direction

The problem is that of a composite pipe made of 3 layers; UPVC, chopped strand mat (CSM) and rovings. Whilst UPVC and CSM are considered to be isotropic, the rovings are unidirectional providing reinforcement in the hoop direction only. Two cases are considered, fully restrained and unrestrained end conditions.

(a) The Unrestrained Case

Equilibrium

$$\frac{PD}{2} = \sigma_{1x} \cdot t_1 + \sigma_{2x} \cdot t_2 + \sigma_{3x} \cdot t_3 \tag{1a}$$

$$\frac{PD}{4} = \sigma_{1y} \cdot t_1 + \sigma_{2y} \cdot t_2 \qquad (\sigma_{3y} = 0) \tag{1b}$$

Compatibility

$$\varepsilon_{1x} = \varepsilon_{2x} = \varepsilon_{3x} = \varepsilon_x \tag{2a}$$

$$\varepsilon_{1y} = \varepsilon_{2y} = \varepsilon_y \tag{2b}$$

Stress–strain relations

For UPVC and CSM

$$\sigma_x = \frac{E}{1-\nu^2}(\varepsilon_x + \nu\varepsilon_y) \tag{3a}$$

$$\sigma_y = \frac{E}{1-\nu^2}(\varepsilon_y + \nu\varepsilon_x) \tag{3b}$$

For the rovings

$$\sigma_{3x} = E_3\varepsilon_x \tag{3c}$$

Solving eqns (1), (2) and (3) gives

$$\varepsilon_x = \frac{PD}{4}\left(\frac{2-\nu}{M_1 - \nu^2 M_2}\right) \tag{4}$$

and

$$\varepsilon_y = \frac{PD}{4\nu M_2}\left(2 - \frac{(2-\nu)M_1}{M_1 - \nu^2 M_2}\right) \tag{5}$$

where

$$M_1 = \frac{1}{1-\nu^2}(E_1t_1 + E_2t_2) + E_3t_3$$

and

$$M_2 = \frac{1}{1-\nu^2}(E_1t_1 + E_2t_2)$$

All Poisson's ratios are taken as being equal to 0·4, and the thicknesses, t, are scaled according to the glass content. The Young's moduli and ultimate strengths used are those of Table 1.

(b) Full Axial Restraint

The analysis is similar to the previous case. Only one equilibrium equation is required, e.g. eqn. (1a), the same compatibility equations can be used with $\varepsilon_y = 0$ and the same stress–strain relations as before. This gives

$$\varepsilon_x = \frac{PD}{2M_1} \tag{6}$$

and

$$\varepsilon_y = 0 \tag{7}$$

The same approach was adopted to obtain a solution for the case of a 4-layer pipe which includes axial rovings; see Table 3 for specimens Nos 8 and 10.